Title: Membrane potential modulates ERK activity and cell proliferation

Authors: Mari Sasaki[1]*, Masanobu Nakahara[1], Takuya Hashiguchi [1], Fumihito Ono [1],

Affiliations:

[1] Department of Physiology, Division of Life Science, Faculty of Medicine, Osaka Medical and Pharmaceutical University; Takatsuki, Osaka, Japan.

*Corresponding author. Email: mari.sasaki@ompu.ac.jp

Summary: Plasma membrane potential has been linked to cell proliferation for over 40 years. In this study, we experimentally demonstrated that membrane depolarization promotes mitosis and that this process depends on the voltage-dependent activation of extracellular signal-regulated kinase (ERK). Notably, ERK activity showed a clear dependence on the membrane potential, independent of growth factor stimulation. This voltage dependence was observed even near the resting membrane potential, indicating that small shifts in the resting potential can influence proliferative activity. Voltage-dependent ERK activity is derived from the altered dynamics of phosphatidylserine and is not mediated by calcium influx from the extracellular space. These findings suggest that fundamental biological processes such as cell proliferation are regulated by the physicochemical properties of membrane lipids. This study highlights the broader physiological roles of membrane potentials beyond action potentials, which are well-established in neural systems.

Introduction:

Plasma membrane potential refers to the voltage difference across a cell's lipid bilayer, which is established by the asymmetric distribution and conductance of intracellular and extracellular ions. These ion gradients are maintained by the combined action of passive and active transport mechanisms involving various ion channels and transporters embedded in the membrane. Although each cell type exhibits a characteristic resting membrane potential, its physiological role has primarily been studied in excitable cells, such as muscle and nerve cells, whereas non-excitable cells have received comparatively little attention (1, 2).

However, accumulating evidence suggests that the physiological relevance of membrane potentials extends beyond action potentials in excitable cells (3). Membrane potential has been implicated in diverse biological processes including embryonic patterning, tissue regeneration, and cancer progression (4). It plays a critical role in establishing left–right asymmetry during early embryogenesis (5). Furthermore, the resting membrane potential has been linked to a cell's proliferative capacity (6-10), with depolarized cells consistently showing increased mitotic activity. In support of this view, Voorhess et al. demonstrated that sustained depolarization promotes DNA synthesis in chick spinal cord neurons (11). These findings align with the observation that oncogenically transformed cells tend to be more depolarized than their normal counterparts (12). Despite numerous reports associating the membrane potential with cell proliferation, the molecular mechanisms underlying this relationship remain unclear.

Cell proliferation is tightly regulated by extracellular growth factors and their downstream intracellular signaling cascades, among which the mitogen-activated protein kinase (MAPK) pathway is central. A key component of this pathway, extracellular signal-regulated kinase

(ERK), plays a crucial role in controlling cell proliferation (13). ERK signaling is frequently upregulated in tumors but downregulated under contact inhibition or in growth-arrested cells (14).

Recent study has shown that phosphatidylserine and K-Ras undergo changes in their nanoscale organization upon plasma membrane depolarization. Voltage-dependent ERK activation occurs when constitutively active K-RasG12V mutant is overexpressed (3). However, the proliferative capacity was not the primary focus of this study, leaving the question of whether voltage-dependent ERK could explain membrane potential-dependent cell proliferation.

In this study, we provide experimental evidence that membrane depolarization enhances mitotic activity and that this effect is associated with voltage-dependent activation of ERK.

Result

Mitotic activity is enhanced by membrane depolarization via the MAPK cascade

Cell proliferation has long been associated to membrane voltage (9). We first examined whether a causal relationship existed between membrane potential and mitotic activity in our experimental system. To specifically monitor the mitotic phase of the cell cycle, U2OS cells were synchronized in the G1 phase by treatment with 2 mM thymidine for 20 h, followed by 8–9 h of normal incubation (G1 release). The cells were subjected to time-lapse imaging (Fig. 1A). Cytokinesis, which was easily identified in bright-field images (Fig. 1B), was quantified in each frame. Cells were maintained in serum-containing medium, except during the phase in which K^+ concentration was altered (Fig. 1A).

The number of mitotic cells increased 14–15 h after G1 release, corresponding to approximately 6 h after the onset of time-lapse imaging (Fig. 1C). Because only a limited number of conditions could be tested per experiment, the control condition (5K) was included for normalization. Mitotic activity, defined as the number of cells undergoing division, was significantly enhanced in cells exposed to 15 mM K^+ (Fig. 1C, D). These results indicated that membrane depolarization promotes mitotic activity, supporting a causal relationship between membrane potential and proliferation. Notably, mitotic activity under $15K^+$ conditions was comparable to that observed under FBS-supplemented conditions (5K+FBS and 15K+FBS). The effects of depolarization and FBS were not additive, suggesting that the proliferative activity plateaued under both conditions.

Next, we investigated the potential involvement of ERK in depolarization-induced mitotic activity. Treatment with the MEK inhibitor U0126 abolished the proliferative effect of 15 mM K^+, indicating that MEK activation plays a pivotal role in depolarization-induced proliferation (Fig. 1C, D).

Together, these findings suggest that MEK–ERK signaling mediates depolarization-induced mitotic activation. However, our results differ from those of a previous report showing that ERK activation occurs only when extracellular potassium exceeds 50 mM in cells expressing wild-type K-Ras (3). Therefore, it remains unclear whether depolarization-induced proliferation is mediated by voltage-dependent ERK activation. To address this, we examined whether ERK could be activated within the physiological range of membrane depolarization.

ERK activity has voltage-dependency within the physiological range of the membrane potential

Although Western blotting is a powerful tool for detecting all-or-nothing phenomena, it is not suitable for quantitatively capturing subtle changes or events with high cell-to-cell variability. Moreover, it is inadequate for analyzing detailed kinetics. To overcome these limitations, we used live-cell imaging. ERK activity was monitored by Förster Resonance Energy Transfer (FRET) imaging using the ERK biosensor EKAREV, while the plasma membrane potential was manipulated by altering the extracellular potassium concentration. EKAREV is an intramolecular FRET biosensor that undergoes conformational changes depending on ERK activity (15). Ypet and ECFP were used as the FRET pair. For simplicity, we will refer to the pair as YFP and CFP, respectively.

When U2OS cells expressing EKAREV were perfused with 145 mM K^+ solution, the YFP/CFP ratio increased over the subsequent 10–20 min, indicating ERK activation (Fig. 2A, B). These kinetics are consistent with those reported previously (3), confirming that our imaging system can capture depolarization-induced ERK activation.

For quantitative analysis, two types of normalization were combined: one to account for variation among dishes and the other for variation among cells. Since the raw YFP/CFP value varied among dishes (Fig.S1), presumably due to the difference in the expression level of the EKAREV probe and the background noise, the YFP/CFP value before application of the high K^+ solution was averaged and used as a reference. The ratio of the raw YFP/CFP value to the reference value was defined as the normalized YFP/CFP value. To normalize variation among cells, cells were stimulated with EGF (10 ng/mL) at the end of the experiment, which presumably yielded a near-saturated YFP/CFP value (ERK activity). This value was used to determine the maximum ERK activity in each cell. We defined % ERK activity as the high K^+-induced ERK activity (relative to the reference) divided by the maximum activity with EGF stimulation. Quantitative analyses were performed on imaged single cells.

Perfusion with 145 mM K^+ strongly activated ERK (Fig. 2A, B), and similar results were observed in HEK293, HeLa, and A431 cells (Fig. S2). The mean ERK activity with 145 mM high K^+ perfusion was unexpectedly close to 100% (Fig.2B), indicating that depolarization induced by 145 mM K^+ had a similar impact on cells as EGF stimulation. Because 145 mM extracellular K^+ is far beyond the physiological range, we next tested more moderate depolarizations. Contrary to a previous report (3), our imaging-based system detected ERK activation with 30 mM K^+, and even with 15 mM K^+—the condition under which mitotic activity was enhanced. Thus, even mild depolarization near the physiological range is sufficient to activate ERK, which may promote cell division. Importantly, as U2OS cells express wild-type K-Ras rather than an oncogenic mutant (16), our results raise the possibility that voltage-dependent ERK activation may also occur in non-transformed cells. The average ERK activity with 30 mM K^+ perfusion was approximately half of the maximum. The average ERK activity was further reduced when perfused with 15 mM K^+ solution (Fig.2B). These results indicate that ERK has voltage-dependent activity not only at extreme depolarization, but also within near-physiological membrane potentials.

An additional advantage of our imaging system is its ability to analyze ERK activity at the single-cell level. When individual cells were examined for the responses, the overall distribution was not Gaussian, and a large proportion of cells perfused with 145 mM K^+ solution showed %ERK activity of 90% or higher (Fig. 2B, C). On the other hand, % ERK activity of cells perfused with 30 mM K^+ solution was concentrated around 50 ~ 60%, and the average response was lower. The variance in response was larger in cells perfused with the 15 mM K^+ solution, with

a significant proportion of cells showing no response (Fig. 2C). The correlation coefficient between the % ERK activity and the logarithm of extracellular K^+ concentration was 0.54 (Fig. 2C). Since membrane potential is proportional to the logarithm of extracellular K^+ (Nernst equation), these data confirm that ERK activity is voltage-dependent across both supraphysiological and physiological ranges.

ERK can be activated by multiple growth factors, as well as by stimuli such as neural excitation and mechanosensory input (17, 18), where extracellular Ca^{2+} entry is sometimes implicated. For instance, ERK activation in neurons is abolished under Ca^{2+}-free conditions (19), and mechanosensory stimulation via Piezo1-mediated Ca^{2+} influx activates ERK. Therefore, we examined whether extracellular Ca^{2+} entry was required for voltage-dependent ERK activation. Perfusion with Ca^{2+}-free 145 mM K^+ solution activated ERK to the same extent as EGF stimulation, indicating that extracellular Ca^{2+} influx is not required (Fig. 2D, E).

Previous studies have reported that ERK is activated in response to hypotonic cell swelling (20, 21). However, under our experimental conditions, no ERK activation was observed at 70% or 50% osmolarity (Fig. S3). We also confirmed that perfusion itself had negligible effects, as no ERK activation was detected upon the initiation of $5K^+$ perfusion (Fig. S3).

ERK activity depends on plasma membrane potential

ERK was previously reported to be activated only above –10mV with wild-type K-Ras (3). To gain further insight into the relationship between voltage-dependent ERK activation and the absolute membrane potential, we employed electrophysiology in combination with live cell imaging**.**

ERK activity was monitored by EKAREV FRET imaging, whereas depolarization was achieved by the voltage-clamp electrophysiology. Because U2OS cells were not amenable to the giga-seal formation required for patch clamping, we used HEK293 cells stably expressing the ERK biosensor, EKAREV.

In a preliminary experiment, we performed whole-cell patch-clamp analysis, but ERK activation was not detected, even upon EGF stimulation, suggesting that the intracellular components necessary for ERK activation were depleted by the whole-cell configuration. Thus, we next turned to the perforated patch-clamp technique using gramicidine, which preserves intracellular components.

HEK293 cells stably expressing EKAREV were depolarized from a holding potential of –80 mV. A control cell with the same optical view and whose membrane voltage was not manipulated is shown in blue (Fig. 3A–F).

Depolarization to –40 mV did not upregulate ERK (Fig.3A and D). Depolarization from –80 mV to –20 mV significantly activated ERK (Fig. 3B and 3E). Depolarization to 0 mV resulted in the strongest ERK activation, which approached the maximum level (Fig. 3C, F).

In our experimental condition, HEK cells exhibited resting membrane potential ranging from –36 mV to –15 mV. This is in line with the lack of ERK activation at –40 mV.

Notably, ERK activity began to decline within 1 min after repolarization to –80 mV, a much faster timescale than the 30 min reported previously (3). The rapid and reversible change in ERK activity coupled with membrane potential contrasts with its activation by EGF, which usually remained sustained for more than 10 min (Fig. 3B-C, E-F).

The correlation coefficient between % ERK activity and membrane potential was 0.54 (Fig.3G), suggesting that ERK activity was voltage-dependent, even near the resting membrane potential. We also confirmed that depolarization to 0 mV alone was sufficient to activate ERK to a level comparable (~88±35%) to EGF stimulation (Fig. 3G).

The variance of % ERK activity was larger at –20 mV compared to either 0 mV or –40 mV depolarization pulses (Fig. 3G). We speculate that this variability arises from differences in the resting membrane potentials of individual cells, which were observed to range between –36 mV and –15 mV. At –20 mV, the extent of depolarization therefore depends on each cell's initial potential: in some cells, the shift produces little or no depolarization, whereas in others it results in substantial depolarization. This variability in the effective voltage change likely accounted for the broader distribution of ERK responses.

MAPK cascade activation upon depolarization

We confirmed ERK activation upon high-K^+ perfusion by Western blotting. In this experiment, we used 145 mM K^+ perfusion, since 50 mM K^+ had previously been reported not to upregulate ERK activity by Western blot (3). U2OS cells were perfused with 145 mM K^+ solution and lysed in lysis buffer. Consistent with our imaging results, ERK was phosphorylated following high-concentration K^+ perfusion (Fig. 4A-B).

Next, we examined whether the upstream components of the canonical MAPK signaling cascade were similarly affected under the same conditions. MEK and c-Raf, both located upstream of ERK, were also phosphorylated by 145 mM K^+ perfusion (Fig. 4A-B). These findings indicate that membrane depolarization activates the MAPK cascade.

Our live-cell imaging data revealed that depolarization-induced ERK activation displays considerably slower kinetics than voltage-gated ion channels, which typically respond within a millisecond (22). Therefore, we investigated the kinetics of upstream MAPK components using imaging-based approaches, which allowed for a more detailed temporal resolution.

Ras was activated upon depolarization with rapid kinetics

Next, we examined the Ras activity upstream of c-Raf. Although Ras nanoclusters are known to activate the downstream MAPK cascade, there is no direct evidence that Ras itself is activated by depolarization. Ras activity was monitored using the FRET-based biosensor Raichu-Ras (23). Raichu-Ras is an intramolecular biosensor that undergoes a conformational change upon Ras activation, resulting in increased FRET efficiency. When FRET occurs, the lifetime of the donor fluorophore decreases. To monitor Ras activity in the plasma membrane, we employed fluorescence lifetime imaging microscopy combined with FRET (FLIM-FRET) (24) and confocal microscopy. U2OS cells expressing Raichu-Ras were perfused with a 145 mM K^+ solution, followed by stimulation with EGF (10 ng/mL).

The mean fluorescence lifetime of the donor fluorophore of Raichu-Ras at the plasma membrane decreased within 2 min after 145 mM K^+ perfusion, indicating Ras activation (Fig. 4C). The activation kinetics were comparable between high K^+ stimulation and EGF stimulation, and were markedly faster than depolarization-induced ERK activation. These results are also consistent with previous reports (3, 25). Taken together, these data suggested that Ras is activated by membrane depolarization with more rapid kinetics than ERK.

The phosphatidylserine dynamics are involved in voltage-dependent ERK activity

Next, we investigated signaling events upstream of Ras. Changes in the membrane potential are expected to occur within milliseconds; thus, upstream events should occur with kinetics that are at least as fast as those of Ras. Plasma membrane depolarization induces the nanoscale reorganization of phosphatidylserine (3). K-Ras, which targets the plasma membrane through electrostatic interactions with phosphatidylserine, undergoes nanoclustering and amplifies MAPK signaling in fibroblasts, neuroblastoma cells, and Drosophila neurons (3). Based on these findings, we examined whether phosphatidylserine nanoclusters contribute to voltage-dependent ERK activation in U2OS cells.

Phosphatidylserine dynamics were monitored by intermolecular FRET using the phosphatidylserine-specific probe LactC2 (Fig. 4D). The C2 domain of lactadherin (LactC2), which binds phosphatidylserine, enables visualization when fused with CFP or YFP (24). The fluorescence lifetime of CFP-LactC2 was 2.375 ± 0.014 ns, which decreased to 2.345 ± 0.013 ns upon co-expression of YFP-LactC2 (Fig. 4E), indicating that phosphatidylserine nanoclustering could be monitored by FLIM-FRET. Importantly, the fluorescence lifetime of CFP-LactC2 in cells co-expressing YFP-LactC2 decreased within 2 min of 145 mM K^+ perfusion, demonstrating depolarization-induced phosphatidylserine nanoclustering (Fig. 4F, 4G). The kinetics of nanoclustering are comparable to those of Ras activation, which is consistent with the notion that phosphatidylserine and Ras interact.

To determine whether phosphatidylserine dynamics were required for voltage-dependent ERK activation, phosphatidylserine was depleted by treating cells with fendiline for 48 h (26). Under these conditions, high K^+-induced ERK activation was markedly reduced (Fig. 4H-I). These findings indicated that phosphatidylserine dynamics are critical for voltage-dependent ERK activation in U2OS cells.

Discussion

The relationship between cell proliferation and the membrane potential has been widely discussed since the 1970s. However, as few studies have addressed the molecular mechanisms involved, the relationship between membrane potential and proliferative capacity remains unclear. Regarding the molecular mechanisms involved, a study conducted in 2015 demonstrated a correlation between MAP activity and membrane potential. However, ERK voltage dependence within the physiological membrane potential range has not yet been demonstrated. Therefore, it remains unclear whether voltage-dependent MAP activation can explain the link between membrane potential and cell proliferation. In this study, we experimentally demonstrated a causal relationship between the membrane potential and mitotic activity (cytokinesis) within the physiological membrane potential range. This effect is associated with depolarization-induced ERK activation via phosphatidylserine dynamics. Thus, we were able to clarify the molecular mechanism of a phenomenon that has long been suggested to be a correlation between membrane potential and proliferative capacity.

We showed that membrane depolarization induces mitotic activity through ERK activation (Fig. 1), indicating that membrane potential is not merely correlated with, but can directly regulate mitotic activity. Some reports have indicated that ERK plays an important role in S phase entry (27), whereas others have proposed a role in mitosis (28-30). Further studies are needed to elucidate which step(s) of the cell cycle are regulated by the membrane potential.

A potential limitation of extracellular K^+-based approaches is their reliance on the Nernst equation to estimate membrane potential, which oversimplifies the actual situation by neglecting voltage-gated ion channel activity and compensatory mechanisms. To directly address this concern, we measured membrane potential using the perforated patch-clamp technique and confirmed that the potential was stable during perfusion with 145 mM K^+ (only a 1–5 mV drift within 20 min). Moreover, we used a voltage clamp to precisely control the membrane potential and demonstrated that ERK activity was directly regulated by the voltage itself, excluding the influence of other secondary factors. An additional strength of electrophysiology is its ability to examine the effects of repolarization, which is difficult to assess with conventional perfusion-based methods owing to slow solution exchange.

A key feature of the ERK response to voltage, compared to EGF stimulation, was the graded relationship between the stimulus and the response (Fig. 2 and 3). Notably, ERK activity is downregulated upon membrane repolarization, but remains active for at least 5 min after growth factor binding (31). This suggests that the membrane potential acts as a fine tuner of ERK, in contrast to growth factor stimulation, which functions more like an on/off switch.

Using FRET-based imaging, we analyzed the kinetics of each step in the signaling pathway. Nanoclustering of phosphatidylserine and subsequent Ras activation occurred within 2 min (Fig. 4C, 4F), whereas ERK activation required more than 5 min (Fig. 2B). This delay is reasonable given that several upstream molecules must be activated before ERK.

Another advantage of imaging-based analysis is the ability to quantitatively measure ERK activity in individual cells. Surprisingly, we found large cell-to-cell variability in depolarization-induced ERK activation. Importantly, such variability is averaged out and is thus invisible in Western blot analysis, which is commonly used to study ERK signaling. Surprisingly, depolarization to 0 mV activated ERK to the same extent as EGF stimulation.

Coupled with electrophysiology, imaging also allows us to monitor ERK activity with a temporal resolution that perfusion or biochemical assays cannot achieve. ERK was activated within 1 min of depolarization and remained elevated for at least 5 min. Deactivation kinetics upon repolarization were similar to those upon activation (Fig. 3).

We also demonstrated that ERK activity exhibits a clear voltage dependence, spanning from the resting membrane potential to states of strong depolarization. This observation is consistent with the idea that voltage-dependent ERK activation arises from changes in phosphatidylserine dynamics in the plasma membrane, which are governed by the fundamental physicochemical properties of the lipid bilayer. Taken together, our findings indicate that plasma membrane potential should be regarded as a previously unrecognized but important regulator of ERK signaling.

In this study, we primarily used U2OS cells because their flat morphology makes them suitable for live-cell FRET imaging. Although cancer cell lines, including U2OS, may display bioelectric properties that differ from those of noncancerous cells, our findings raise the possibility that voltage-dependent ERK activation is a fundamental and broadly applicable phenomenon rather than a feature specific to osteosarcoma cells. This conclusion is supported by the fact that essential components of this pathway, namely phosphatidylserine, Ras, and MAPK (including ERK), are ubiquitously expressed in mammalian cells. Consistent with this finding, we observed voltage-dependent ERK activation across multiple cell lines: U2OS, HeLa, HEK293, and A431 cells (Fig.S2). These observations indicate that the mechanism we describe is not cell-type-restricted, but rather a universal property of mammalian cells.

Zhou et al. reported that phosphatidylserine and PIP_2 undergo nanoscale reorganization upon plasma membrane depolarization (3). K-Ras also changes its nanoscale organization through electrostatic interactions between its basic residues and anionic phosphatidylserine (3, 32). Such interactions may also occur between clusters of basic amino acids in other proteins and anionic phospholipids such as phosphatidylserine or PIP_2. For example, a cluster of basic residues in EGFR interacts with PIP_2, and clustering of EGFR leads to its activation (33, 34). This suggests that EGFR activity may also be regulated by the membrane potential. Several other proteins interact with PIP_2 and contain clusters of basic residues, suggesting that the membrane potential regulates a broad range of proteins and, thereby, many physiological processes.

We showed that the membrane potential modulated phosphatidylserine dynamics (Fig. 4F and G). The relationship between electrostatic potential and membrane organization has been discussed previously (35). Transmembrane potential affects the lateral sorting of membrane components, as well as the positioning of polar lipid headgroups (35). In addition, membrane lipid viscosity, which depends on lipid/protein composition and organization, can be altered by voltage (36-38). However, the precise mechanism through which transmembrane potentials modulate lipid and protein organization remains unclear.

Overall, our results link three elements—plasma membrane voltage, ERK activity, and cell proliferation—and propose a new signaling cascade that regulates cell division. These findings suggest that ion channels and transporters that regulate membrane potential are potential therapeutic targets for cancer. Moreover, because ERK is involved in differentiation, migration, senescence, and apoptosis (39), the membrane potential may also regulate these processes, representing additional opportunities for drug development.

What is the biological significance of membrane potential regulation in cell proliferation? The stochastic ERK activation reported by Aoki et al. may result from fluctuations in membrane potential (40). Furthermore, intercellular propagation of membrane potential via gap junctions can increase ERK activity and synchronize proliferation (40). Such synchronized proliferation could be advantageous in tissues such as the epithelium. Our finding that membrane potential acts as an analog modulator of ERK activity is consistent with this hypothesis and may enable the nuanced regulation of cell proliferation.

It is now evident that the physiological significance of membrane potential extends beyond ion channel function. Given that the membrane potential is a physical property that influences all cellular components, including proteins and lipids, many additional biological phenomena regulated by voltage remain to be explored.

Acknowledgments:

We thank Dr. Michiyuki Matsuda (Kyoto University) for providing the EKAREV and RaichuEV-HRas plasmids. We thank Dr. Michiyuki Matsuda, Dr. Tohru Ishitani, and Dr. Jianmin Cui for critically reading this manuscript. **Funding:** KAKENHI 20K07268 to M.S. Naito Foundation to M.S. Takeda Science Foundation to M.S.

Author contributions:

Conceptualization: MS
Data curation: MS
Formal analysis: MS,MN
Funding acquisition: MS

Investigation: MS, TH
Methodology: MS
Project administration: MS
Software: MS, MN
Writing—original draft: MS
Writing—review & editing: MS, FO

Declaration of interests: The authors declare no competing interests.

Material and Methods

Plasmid and reagents

The expression vectors for the EKAREV and Raichu-Ras plasmids were kindly provided by Dr. Michiyuki Matsuda (Kyoto University). mRFP-Lact-C2 was a gift from Sergio Grinstein (Addgene plasmid # 74061 ; http://n2t.net/addgene:74061 ; RRID:Addgene_74061)(24). YFP-LactC2 and CFP-LactC2 were generated from the mRFP-LactC2 plasmid by exchanging mRFP with YPet and SECFP, respectively. Recombinant human EGF was purchased from Thermo Fisher Scientific. Fendiline was purchased from CAYMAN Chemicals. Gramicidin was purchased from Sigma-Aldrich.

Cells

U2OS cells were purchased from the European Collection of Authenticated Cell Cultures and maintained in McCoy's 5A medium supplemented with 10% fetal bovine serum. HEK293 cells stably expressing EKAREV were generated by PiggyBac transposon system transfection with EKAREV/pPBbsr2 and mPBase/pCMV vectors and were maintained in DMEM medium supplemented with 10% fetal bovine serum. Cells were cultured in a 5% CO_2-humidified environment at 37°C.

Time-lapse imaging with high K^+ perfusion

U2OS cells were plated on a glass-based dish (Matsunami) and transfected with the EKAREV plasmid using the TransIT-LT1 reagent (Mirus) according to the manufacturer's instructions. The cells were serum starved for 3–16 h before time-lapse FRET imaging. The cells were imaged using an inverted microscope (Ti2-E; Nikon) equipped with a 60× objective (NA=1.4; Nikon), a CMOS camera (Zyla4.2; Andor), and an LED illumination system (xCite Xylis; Excelitas Technologies). A W-VIEW GEMINI image-splitting system (Hamamatsu Photonics) was used to acquire the CFP and YFP images simultaneously. The following filters and dichroic mirrors were used: 439/24 for excitation; 483/32 (CFP) and 542/27 (YFP) for emission; and FF509-fDi01 for the dichroic mirror. FLIM-FRET images were acquired using a Stellaris (Leica) confocal microscope with excitation at 448 nm. The fluorescence lifetime of the donor fluorophore was measured at 460–500 nm with a pinhole size of 1 AU, so that only signals from the plasma membrane were detected. The perfusion solution was changed using a valve-controlled gravity perfusion system (VC3-4PG) controlled by an Arduino. The solutions used were as follows (in mM), 5 K; 140 NaCl, 5 KCl, 1 $CaCl_2$, and 1 $MgCl_2$. 15K ; 130 NaCl, 15 KCl, 1 $CaCl_2$, 1 $MgCl_2$. 30K; 115 NaCl, 30 KCl, 1 $CaCl_2$, 1 $MgCl_2$. 145K ; 145 KCl, 1 $CaCl_2$, 1 $MgCl_2$. 5K (Ca free); 140 NaCl, 5 KCl, 1 EGTA, 1 $MgCl_2$. 145K (Ca free) ; 145 KCl, 1 EGTA 1 $MgCl_2$. All solutions contained 20 mM HEPES (pH 7.4). The osmolarity was adjusted to 296–305 mOsm/L using glucose. The EGF solution was prepared using a low-K^+ solution (5 mM K^+).

Patch clamping

HEK293 cells stably expressing EKAREV were plated on a glass-based dish (Matsunami) and serum starved for 16 h before the start of the experiment. The gramicidin-perforated patch-clamp experiment was performed using a Multiclamp 700 B amplifier (Digidata 1440A) and pClamp software (Axon). Gramicidin (60 μg/mL) in a patch solution (145 mM KCl, 5 mM EGTA, 10 mM HEPES pH7.4) was sonicated for 5 min and backfilled into the patch pipette. The 5K solution was used as the external patch solution. FRET images were acquired using a confocal microscope LSM510Meta (Ziess) excited at 458 nm. The filters used for CFP and YFP were 475–525 and LP530, respectively. We set the potential to –80mV immediately after the giga-seal formation and waited for at least 5 min to allow pore formation by gramicidin. We started imaging only after membrane potential was expected to have reached a steady state at –80 mV.

Imaging Analysis

Dead and unhealthy cells that did not respond to EGF stimulation were excluded from the analysis. The average intensity of multiple background ROIs was used as the background and subtracted from each image. The fluorescence intensities of the YFP and CFP channels were averaged for each cell and the results were exported as a CSV file. YFP/CFP values were calculated using Excel and R Studio for the patch-clamp and high-K^+ perfusion experiments, respectively. The % ERK activity was calculated by dividing the maximum normalized YFP/CFP ratio after high K^+ perfusion or depolarization by the maximum normalized YFP/CFP ratio after EGR perfusion for each cell. For FLIM-FRET experiments, the average fluorescence lifetime was calculated for each cell. The average fluorescence lifetime of the first 10 min was used as a reference. The normalized fluorescence lifetime was defined as the ratio of the fluorescence lifetime to the reference value. All image analyses were performed using ImageJ software.

Western blot

The following antibodies were used for Western blotting: total ERK (SC514302; Santa Cruz Biotechnology), phospho-ERK (4370; Cell Signaling Technology), total MEK (4394; Cell Signaling Technology), phospho-MEK (2338; Cell Signaling Technology), total c-Raf (9422; Cell Signaling Technology), phospho-c-Raf (CST9431). Cells were lysed in 50 mM Tris (pH 7.5), 150 mM NaCl, 1 mM EDTA, 1% NP40 with protease and phosphatase inhibitor cocktail (Thermo Scientific), 1 mM sodium orthovanadate. Protein samples (10 mg per lane) were separated by SDS-PAGE, immunoblotted onto polyvinylidene fluoride (PVDF) membranes, and detected by ECL using a charge-coupled device (CCD) camera. Quantification was performed using the ImageJ software.

Mitosis analysis

U2OS cells were synchronized in the G1 phase by treatment with 2 mM thymidine for 20 h. Time-lapse imaging was conducted 8–9 h after G1 release using an inverted confocal microscope (Stellaris, Leica) with a 20× objective (NA=0.75) in DIC mode. Images were obtained every 10 min in solutions with different K^+ concentrations without serum (Fig.1A). The number of mitotic cells was counted in each frame. The FBS condition included 10% FBS.

Statistical Analysis

Statistical analyses were performed using R Studio. The level of statistical significance is indicated by asterisks: ns, $p > 0.05$; * $p < 0.05$; ** $p < 0.01$; *** $p < 0.001$; **** $p < 0.0001$.

Fig.1 Mitotic activity is upregulated by membrane depolarization.

(A) Experimental diagram. (B) Representative images showing morphological changes of a U2OS cell before, during, and after cell division. Time (min) indicated relative to the cytokinesis. Scale bar is 10 μm. (C) Mitotic cell counts were accumulated every 1.5 h, normalized by the number of mitotic cells in the first 1.5 h with 5K solution from the same experiment and plotted against time after the start of time-lapse imaging. U; U0126, FBS; 10% FBS. Data are mean±SEM (D) Mitotic cell counts were accumulated for 6 h and normalized by the accumulated number of mitotic cells in 5K solution from the same experiment. 5K vs. 15K p=0.016 (one sample t-test), 5K vs. 5K+FBS p=0.041 (one sample t-test), 5K vs. 15K+FBS p=0.0094 (one sample t-test), 15K vs. 15K+U p=0.0040 (paired t-test). Data are from 13 (for 5K), 13 (for 15K), 7 (for 5K+U), 11 (for 15K+U), 7 (for 5K+FBS) and 7 (for 15K+FBS) independent experiments respectively. Approximately 100–900 mitotic cells were observed within 6 h in each experiment.

Fig.2 ERK is activated upon high K+ perfusion.

(A) YFP/CFP ratio images at the indicated time points. Serum starved U2OS cells expressing EKAREV were perfused with 145 mM high K^+ solution at 10 min, followed by the addition of 10 nM EGF at 30 min. Scale bar is 10 μm. The color scale indicates YFP/CFP ratio. (B) ERK activity with high K^+ perfusion. Serum-starved cells were treated with various concentrations of K^+ solution at 10 min, followed by the addition of 10 nM EGF at 30 min. Normalized % ERK (response by high K / response by EGF; see in the text) activity was calculated as follows: the normalized YFP/CFP (see in the text) was divided by the normalized maximum YFP/CFP after subtracting the mean normalized YFP/CFP at 8–10 min. Data are mean±SEM. Data are from 16, 15, and 23 cells from 3, 4 and 6 independent experiments, for $145K^+$, $30K^+$ and $15K^+$, respectively. (C) The relationship between the logarithm of K^+ concentration and the % ERK activity. R is Pearson's correlation coefficient. The gray area is 95% confidence interval. p=0.00013 (Kruskal-Wallis). N are the same as in (B). (D) Mean normalized YFP/CFP ratio perfused with Ca^{2+} free 145 K^+ high K solution. Starved cells were incubated with $5K^+$ (Ca^{2+} free) solution, followed by perfusion with 145mM K^+ (Ca^{2+} free) solution at 10 min. At 30 min,10 nM EGF was added. Data are mean±SEM. N=14 from 2 independent experiments. (E) The % ERK activity in the Ca(+) and Ca(-) solution. The data for Ca(+) were the same as in Fig.2C($145K^+$). p=0.82 (Wilcoxon rank sum exact test)

Fig.3 ERK activity depends on membrane voltage

(A to C) Mean normalized YFP/CFP ratio. Starved cells were depolarized from a holding potential of –80mV to depolarized membrane potentials (–40, –20 and 0 mV for A, B, and C, respectively) at 5 min, followed by repolarization to –80mV at 10 min. At 15 min, 10 nM EGF was perfused. Data are mean±SD. N=4, 8 and 10 from 2, 5 and 6 independent experiments for –40, –20 and 0 mV, respectively. (D to F) Average normalized YFP/CFP ratio for the first 5 min (–80mV), maximum normalized YFP/CFP ratio at depolarized phase (–40, –20 and 0mV for A, B, and C, respectively), minimum normalized YFP/CFP ratio at repolarized phase (–80mV) and maximum normalized YFP/CFP ratio at EGF stimulated phase (EGF), respectively. Data are mean±SEM. The p–values were calculated using Student's t test. (G) The relationship between

membrane potential and % ERK activity. p=0.0042 (Kruskal-Wallis). R is Pearson's correlation coefficient. The gray area is 95% confidence interval.

Fig.4 The molecular mechanism regulating depolarization-induced mitosis.

(A) Immunoblot analysis of cells perfused with 145K$^+$ solution. (B) Quantification of relative mean band intensity of pERK, pMEK and pcRaf from independent experiments conducted as in (A). Data are mean±SD. (C) Ras activity was monitored by FLIM-FRET imaging. The donor (mTurquoise-GL) lifetime of U2OS cells expressing Raichu-Ras at the indicated time point. The experimental condition was the same as in Fig. 2A. Data are mean±SEM. N= 17 from 4 independent experiments. (D) Schema of intermolecular FRET experiment. Phosphatidylserine clustering was monitored by FLIM-FRET imaging of U2OS cells co-expressing CFP-LactC2 and YFP-LactC2. (E) The fluorescence lifetime of CFP-LactC2. The fluorescence lifetime of CFP-LactC2 decreased when YFP-LactC2 was co-expressed in the same cells. p=0.00080 (Welch Two Sample t-test) N= 25 and 16 from 6 and 5 independent experiments, for CFP-LactC2 alone and co-expressing CFP-LactC2 and YFP-LactC2, respectively. (F) The normalized fluorescence lifetime of CFP-LactC2 was measured at the indicated time point. The experimental condition was the same as in Fig.2A except the EGF stimulation. Data are mean±SEM. N=25 from 6 independent experiments. (G) CFP-LactC2 lifetime images at the indicated time points. The experimental condition is described above. Scale bar is 10 μm. The color scale indicates CFP-LactC2 lifetime. (H) Mean normalized YFP/CFP ratio from phosphatidylserine-depleted starved cells treated with 145 K$^+$ solution at 10 min, followed by the addition of 10 nM EGF. Data are mean±SEM. N=27 from 8 independent experiments. (I) The % ERK activity with or without Fendiline treatment. The data for Fendiline(-) were the same as in Fig.2C(145K+). p=4.4e-9(Wilcoxon rank sum exact test).

References

1. A. L. Hodgkin, A. F. Huxley, The components of membrane conductance in the giant axon of Loligo. *The Journal of Physiology* **116**, 473-473 (1952).
2. E. Neher, B. Sakmann, Single-channel currents recorded from membrane of denervated frog muscle fibres. *Nature 1976 260:5554* **260**, 799-802 (1976).
3. Y. Zhou *et al.*, Membrane potential modulates plasma membrane phospholipid dynamics and K-Ras signaling. *Science* **349**, 873-876 (2015).
4. M. Levin, Bioelectric signaling: Reprogrammable circuits underlying embryogenesis, regeneration, and cancer. *Cell* **184**, 1971-1989 (2021).
5. M. Levin, T. Thorlin, K. R. Robinson, T. Nogi, M. Mercola, Asymmetries in H+/K+-ATPase and cell membrane potentials comprise a very early step in left-right patterning. *Cell* **111**, 77-89 (2002).
6. S. Sundelacruz, M. Levin, D. L. Kaplan, Role of membrane potential in the regulation of cell proliferation and differentiation. *Stem Cell Reviews and Reports* **5**, 231-246 (2009).
7. D. J. Blackiston, K. A. McLaughlin, M. Levin, Bioelectric controls of cell proliferation: Ion channels, membrane voltage and the cell cycle. *Cell Cycle* **8**, 3527-3536 (2009).

8. C. D. Cone, M. Tongier, Contact inhibition of division: Involvement of the electrical transmembrane potential. *Journal of Cellular Physiology* **82**, 373-386 (1973).
9. C. D. Cone, Unified theory on the basic mechanism of normal mitotic control and oncogenesis. *Journal of Theoretical Biology* **30**, 151-181 (1971).
10. R. Binggeli, R. C. Weinstein, Membrane potentials and sodium channels: Hypotheses for growth regulation and cancer formation based on changes in sodium channels and gap junctions. *Journal of Theoretical Biology* **123**, 377-401 (1986).
11. M. L. Voorhess, M. J. Stuart, J. A. Stockman, F. A. Oski, J. Pediatr, Induction of Mitosis in Mature Neurons in Central Nervous System by Sustained Depolarization. *Science* **192**, 155-158 (1976).
12. S. Tokuoka, H. Morioka, The Membrane Potential of the Human Cancer and Related Cells (I). *Gann* **48**, 353-354 (1957).
13. G. Pages *et al.*, Mitogen-activated protein kinases p42mapk and p44mapk are required for fibroblast proliferation (protein kinase cascade/kinase antiense/dominant neptve mutants/growth control/H-killing selection). *Proc. Natl. Acad. Sci. USA* **90**, 8319-8323 (1993).
14. J. Wayne, J. Sielski, A. Rizvi, K. Georges, D. Hutter, ERK regulation upon contact inhibition in fibroblasts. *Molecular and Cellular Biochemistry* **286**, 181-189 (2006).
15. N. Komatsu *et al.*, Development of an optimized backbone of FRET biosensors for kinases and GTPases. *Molecular Biology of the Cell* **22**, 4647-4656 (2011).
16. M. Libert *et al.*, Stress granules are not present in Kras mutant cancers and do not control tumor growth. *EMBO Reports* **25**, 4693-4693 (2024).
17. C. D. Harvey *et al.*, A genetically encoded fluorescent sensor of ERK activity. *Proceedings of the National Academy of Sciences of the United States of America* **105**, 19264-19269 (2008).
18. F. Crozet, R. Levayer, Emerging roles and mechanisms of ERK pathway mechanosensing. **80**, 355-355 (2023).
19. J. C. Corvol *et al.*, Depolarization activates ERK and proline-rich tyrosine kinase 2 (PYK2) independently in different cellular compartments in hippocampal slices. *Journal of Biological Chemistry* **280**, 660-668 (2005).
20. F. Schliess, R. Schreiber, D. Haussinger, Activation of extracellular signal-regulated kinases Erk-1 and Erk-2 by cell swelling in H4IIE hepatoma cells. *Biochemical Journal* **309**, 13-17 (1995).
21. J. Sadoshima, Z. Qiu, J. P. Morgan, S. Izumo, Tyrosine kinase activation is an immediate and essential step in hypotonic cell swelling-induced ERK activation and c-fos gene expression in cardiac myocytes. *EMBO Journal* **15**, 5535-5546 (1996).
22. F. Bezanilla, The voltage sensor in voltage-dependent ion channels. *Physiological Reviews* **80**, 555-592 (2000).
23. N. Mochizuki *et al.*, Spatio-temporal images of growth-factor-induced activation of Ras and Rap1. *Nature 2001 411:6841* **411**, 1065-1068 (2001).
24. T. C. U. s. D. y. s. p. Yeung *et al.*, Membrane phosphatidylserine regulates surface charge and protein localization. **319**, 210-213 (2008).
25. H. Murakoshi *et al.*, Single-molecule imaging analysis of Ras activation in living cells. *Proceedings*

of the National Academy of Sciences of the United States of America **101**, 7317-7322 (2004).

26. K.-j. Cho *et al.*, Inhibition of Acid Sphingomyelinase Depletes Cellular Phosphatidylserine and Mislocalizes K-Ras from the Plasma. **36**, 363-374 (2016).
27. J. G. Albeck, G. B. Mills, J. S. Brugge, Frequency-modulated pulses of ERK activity transmit quantitative proliferation signals. *Molecular cell* **49**, 249-261 (2013).
28. P. S. Shapiro *et al.*, Activation of the MKK/ERK pathway during somatic cell mitosis: Direct interactions of active ERK with kinetochores and regulation of the mitotic 3F3/2 phosphoantigen. *Journal of Cell Biology* **142**, 1533-1545 (1998).
29. F. S. Willard, M. F. Crouch, MEK, ERK, and p90RSK are present on mitotic tubulin in Swiss 3T3 cells: A role for the MAP kinase pathway in regulating mitotic exit. *Cellular Signalling* **13**, 653-664 (2001).
30. E. Iwamoto *et al.*, ERK Plays a Role in Chromosome Alignment and Participates in M-Phase Progression. *Journal of Cellular Biochemistry* **117**, 1340-1351 (2016).
31. A. Kiyatkin, I. K. Van Alderwerelt Van Rosenburgh, D. E. Klein, M. A. Lemmon, Kinetics of receptor tyrosine kinase activation define ERK signaling dynamics. *Sci. Signal* **13**, 5267-5267 (2020).
32. Y. Zhou, J. F. Hancock, Ras nanoclusters: Versatile lipid-based signaling platforms. *Biochimica et biophysica acta* **1853**, 841-849 (2015).
33. Y. Wang *et al.*, Regulation of EGFR nanocluster formation by ionic protein-lipid interaction. *Cell Research* **24**, 959-976 (2014).
34. K. B. A. Halim, H. Koldsø, M. S. P. Sansom, Interactions of the EGFR juxtamembrane domain with PIP2-containing lipid bilayers: Insights from multiscale molecular dynamics simulations. *Biochimica et Biophysica Acta - General Subjects* **1850**, 1017-1025 (2015).
35. J. Malinsky, W. Tanner, M. Opekarova, Transmembrane voltage: Potential to induce lateral microdomains ☆. 10.1016/j.bbalip.2016.02.012 (2016).
36. P. S. O'Shea, S. Feuertstein-Thelen, A. Azzi, Membrane-potential-dependent changes of the lipid microviscosity of mitochondria and phospholipid vesicles. *Biochemical Journal* **220**, 795-801 (1984).
37. P. Herman, J. Malinsky, J. Plasek, J. Vecer, Pseudo Real-Time Method for Monitoring of the Limiting Anisotropy in Membranes. *JOFL] Journal of Fluorescence* **14** (2004).
38. G. Grossmann, M. Opekarová, J. Malinsky, I. Weig-Meckl, W. Tanner, Membrane potential governs lateral segregation of plasma membrane proteins and lipids in yeast. *EMBO Journal* **26**, 1-8 (2007).
39. Y. Sun *et al.*, Signaling pathway of MAPK/ERK in cell proliferation, differentiation, migration, senescence and apoptosis. *Journal of Receptors and Signal Transduction* **35**, 600-604 (2015).
40. K. Aoki *et al.*, Stochastic ERK activation induced by noise and cell-to-cell propagation regulates cell density-dependent proliferation. *Molecular Cell* **52**, 529-540 (2013).

Fig. S1 Non-normalized YFP/CFP ratio responded to high K^+ perfusion.

Serum-starved U2OS cells expressing EKAREV were perfused with a 145 mM K^+ solution at 10 min, followed by the addition of 10 nM EGF at 30 min. Data were obtained from three independent experiments and were not normalized.

Fig. S2 ERK was activated by high K^+ perfusion in multiple cell types

ERK activity after high K^+ perfusion in HEK293 (A), HeLa(B), and A431(C) cells. Serum-starved cells expressing EKAREV were perfused with 145 mM high K^+ solution at the arrow. Data are mean±SEM.

Fig. S3 ERK was not activated by perfusion nor hypotonic shock.

Serum-starved cells expressing EKAREV were perfused sequentially with 5 mM K^+ and a hypotonic solution at the time points indicated by the arrows. 70% and 50% osmolarity correspond to 215 mOsm/L and 155 mOsm/L, respectively. Data are mean±SEM.

A

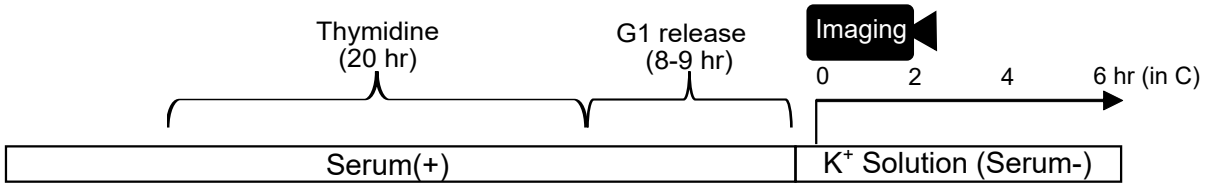
Thymidine
(20 hr)
G1 release
(8-9 hr)
Imaging
0
2
4
6 hr (in C)
Serum(+)
K+ Solution (Serum-)

B

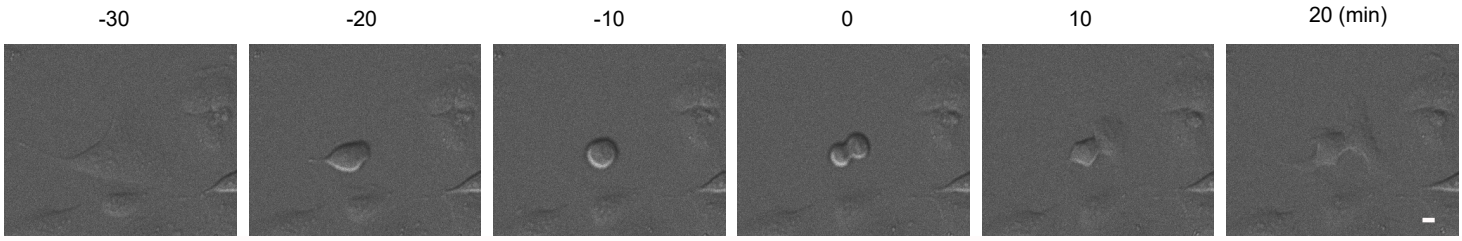
-30
-20
-10
0
10
20 (min)

C

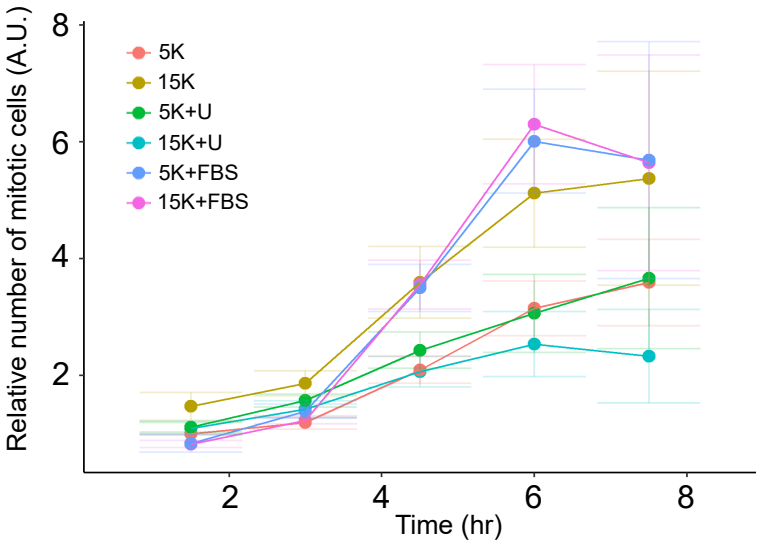
Relative number of mitotic cells (A.U.)
8
6
4
2
5K
15K
5K+U
15K+U
5K+FBS
15K+FBS
2
4
6
8
Time (hr)

D

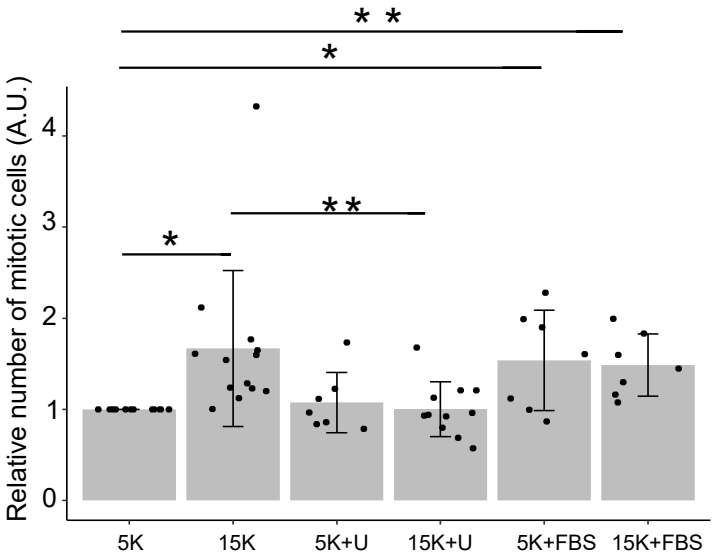
* *
*
**
*
Relative number of mitotic cells (A.U.)
4
3
2
1
0
5K
15K
5K+U
15K+U
5K+FBS
15K+FBS

Fig1

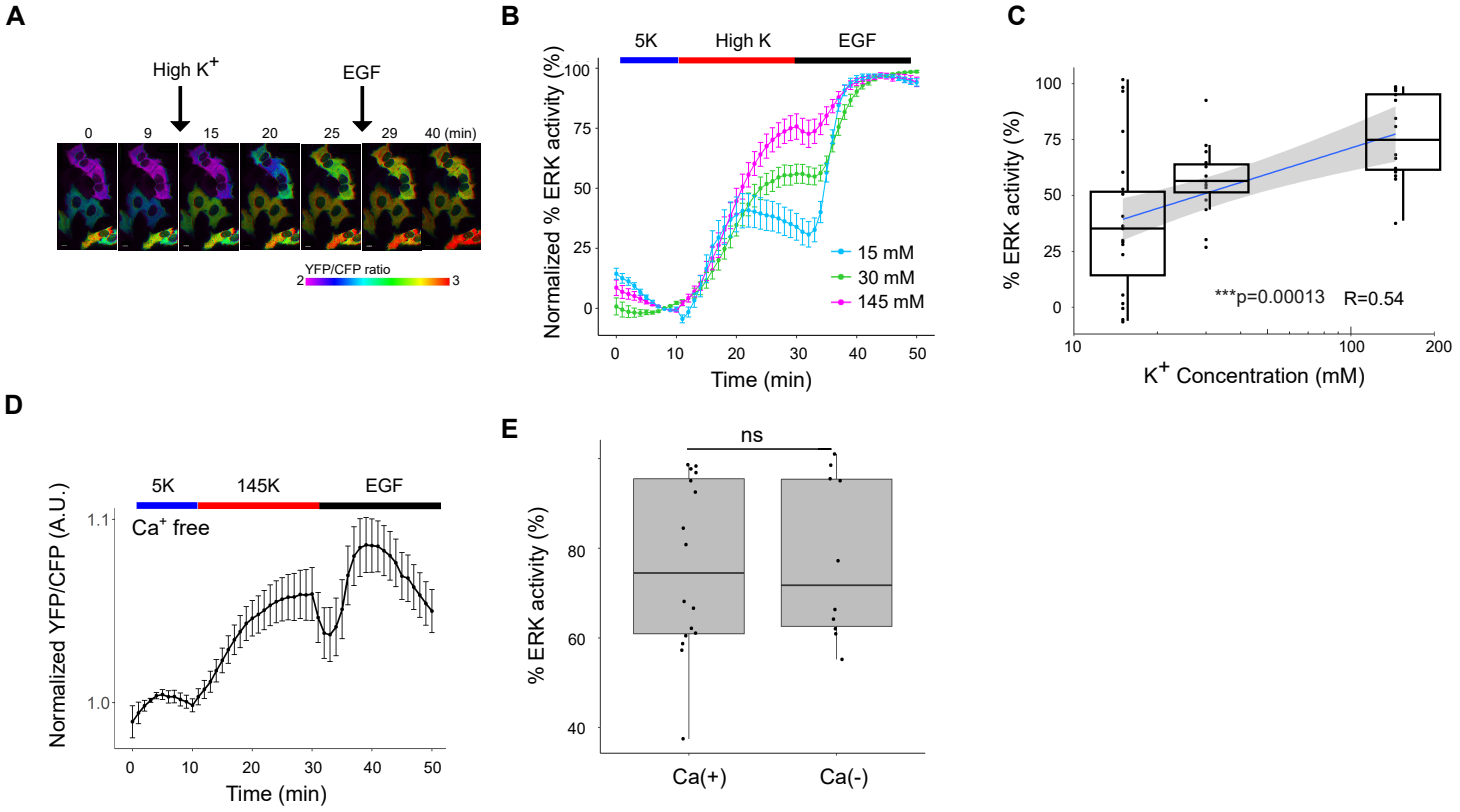
A
High K+
EGF
0
9
15
20
25
29
40 (min)
YFP/CFP ratio
2
3
B
5K
High K
EGF
Normalized % ERK activity (%)
Time (min)
15 mM
30 mM
145 mM
C
% ERK activity (%)
***p=0.00013
R=0.54
K+ Concentration (mM)
D
5K
145K
EGF
Ca+ free
Normalized YFP/CFP (A.U.)
Time (min)
E
ns
% ERK activity (%)
Ca(+)
Ca(-)

Fig.2

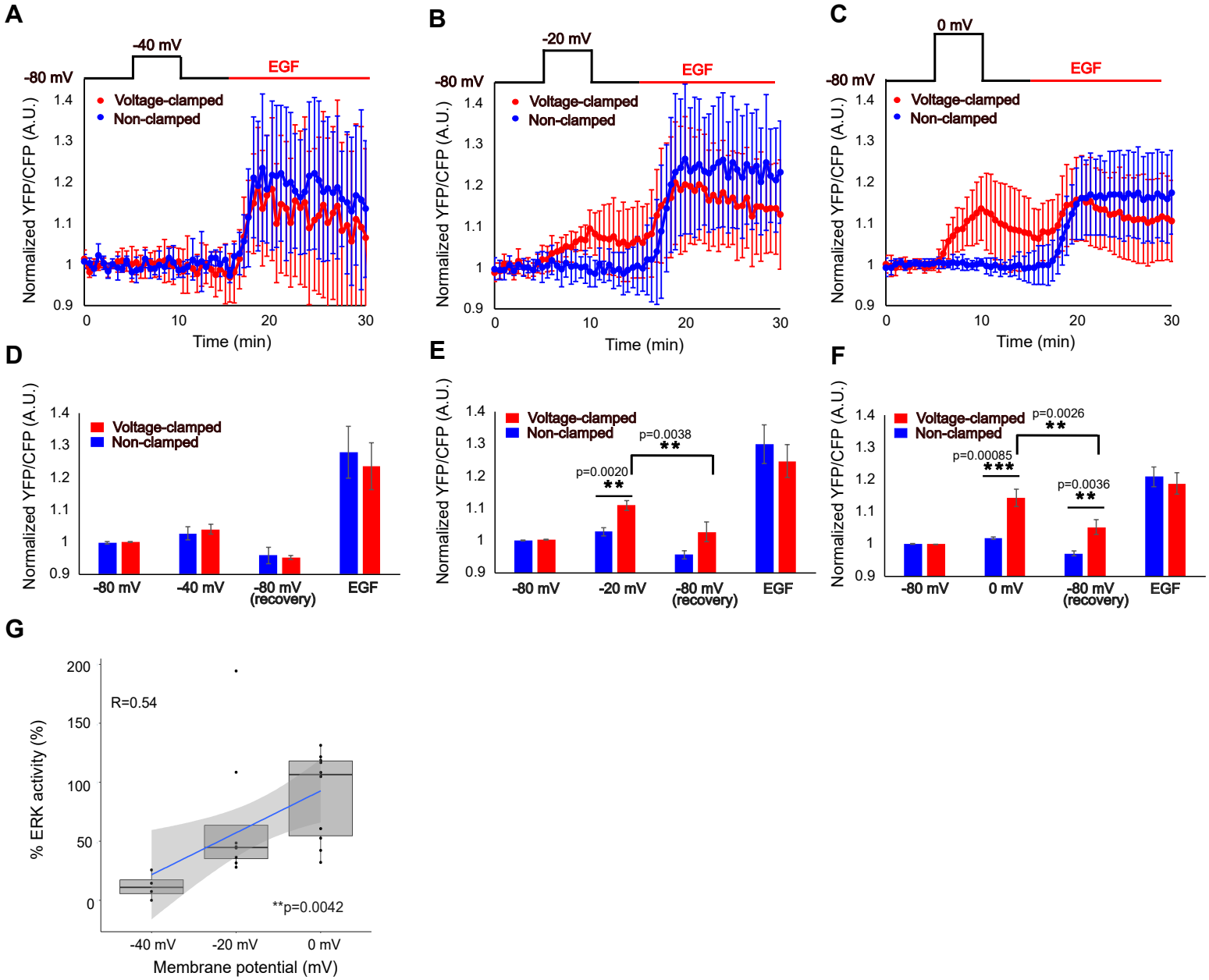
A
-40 mV
-80 mV
EGF
Voltage-clamped
Non-clamped
Normalized YFP/CFP (A.U.)
Time (min)
B
-20 mV
-80 mV
EGF
Voltage-clamped
Non-clamped
Normalized YFP/CFP (A.U.)
Time (min)
C
0 mV
-80 mV
EGF
Voltage-clamped
Non-clamped
Normalized YFP/CFP (A.U.)
Time (min)
D
Voltage-clamped
Non-clamped
Normalized YFP/CFP (A.U.)
-80 mV
-40 mV
-80 mV (recovery)
EGF
E
Voltage-clamped
Non-clamped
p=0.0020
**
p=0.0038
**
Normalized YFP/CFP (A.U.)
-80 mV
-20 mV
-80 mV (recovery)
EGF
F
Voltage-clamped
Non-clamped
p=0.00085
***
p=0.0026
**
p=0.0036
**
Normalized YFP/CFP (A.U.)
-80 mV
0 mV
-80 mV (recovery)
EGF
G
R=0.54
**p=0.0042
% ERK activity (%)
-40 mV
-20 mV
0 mV
Membrane potential (mV)

Fig.3

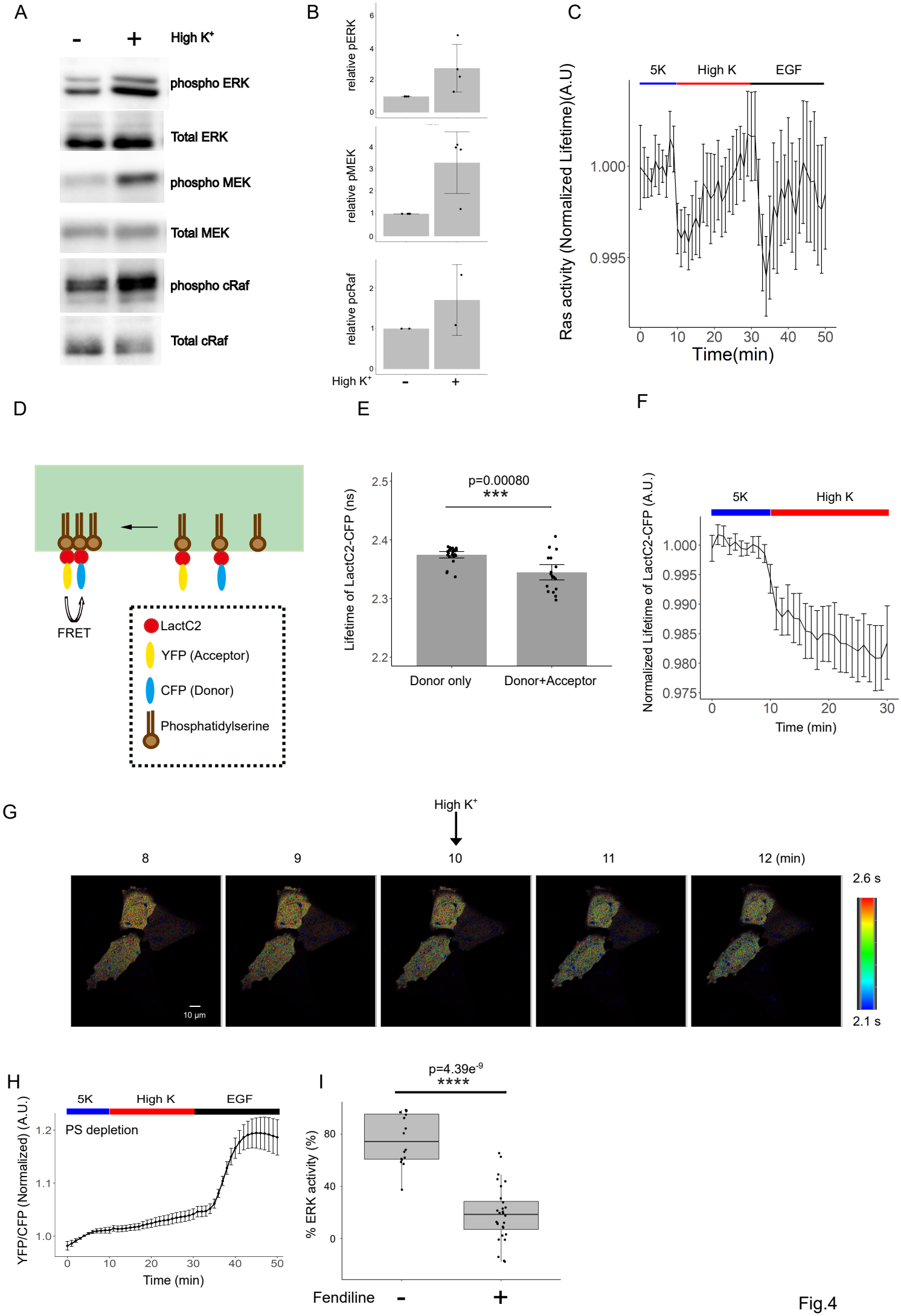
A
-
+
High K+
phospho ERK
Total ERK
phospho MEK
Total MEK
phospho cRaf
Total cRaf
B
relative pERK
relative pMEK
relative pcRaf
High K+
-
+
C
5K
High K
EGF
Ras activity (Normalized Lifetime)(A.U)
1.000
0.995
0
10
20
30
40
50
Time(min)
D
FRET
LactC2
YFP (Acceptor)
CFP (Donor)
Phosphatidylserine
E
p=0.00080
***
Lifetime of LactC2-CFP (ns)
2.5
2.4
2.3
2.2
Donor only
Donor+Acceptor
F
5K
High K
Normalized Lifetime of LactC2-CFP (A.U.)
1.000
0.995
0.990
0.985
0.980
0.975
0
10
20
30
Time (min)
G
High K+
8
9
10
11
12 (min)
2.6 s
2.1 s
10 µm
H
5K
High K
EGF
PS depletion
YFP/CFP (Normalized) (A.U.)
1.2
1.1
1.0
0
10
20
30
40
50
Time (min)
I
p=4.39e-9
****
% ERK activity (%)
80
40
0
Fendiline
-
+

Fig.4